Oceanic Teleconnections: Remote Response to Decadal Wind Forcing

PAOLA CESSI

Scripps Institution of Oceanography, University of California, San Diego, La Jolla, California

PANTXIKA OTHEGUY

E.N.S.T.A., Paris, France

(Manuscript received 15 July 2002, in final form 4 February 2003)

ABSTRACT

The transhemispheric and interbasin response to time-dependent wind forcing localized in the Northern Hemisphere of a single basin is examined using the reduced-gravity shallow-water equations in domains of simple geometry. On decadal timescales, the pressure on the eastern boundary fluctuates synchronously in both hemispheres and thus communicates a signal to latitudes distant from the forcing. The signal then penetrates into the interior through westward radiation of Rossby waves. Associated with the eastern boundary pressure fluctuation is a time-dependent mass flux across the equator that, in a single basin, is balanced by a storage of mass in the unforced hemisphere. Two oceanic basins connected by a reentrant channel at the high-latitude edge of the Southern Hemisphere are then considered. Again the forcing is confined to the Northern Hemisphere of one basin only. In this geometry the time-dependent mass flux across the equator of the forced basin is not entirely balanced within the same basin, but induces a mass flux into the unforced basin, while the mass heaving within the periodic channel is negligible. This process is illustrated by considering winds oscillating at a period on the same order as the Rossby wave transit time in high latitudes. The interhemispheric and interbasin teleconnection is achieved by a combination of long Rossby waves and large-scale, low-frequency gravity waves forced by the Rossby signal. These disturbances share no characteristics of Kelvin waves; that is, they are not boundary trapped.

1. Introduction

This work concerns the decadal and longer response of the oceanic circulation to changes in the wind forcing. Decadal timescales have a special significance in oceanography, since they coincide with the time for baroclinic adjustment of geostrophic flow, mediated by oceanic Rossby waves.

For example, a surprisingly large fraction of the sea level signal at decadal frequencies can be explained by the Rossby wave response of a single baroclinic vertical mode to wind-curl forcing [see Sturges and Hong (2000) for a review of decadal variability of sea level]. The decadal sea level signal is of order a few centimeters, of similar magnitude to the global trend of 2 cm (10 yr)$^{-1}$.

The notion that the upper-ocean signal at a given location might be the result of forcing to the east and subsequent westward propagation as Rossby waves, and not just due to local forcing, is a familiar one. It is less intuitive that in the low-frequency band, where Rossby waves control the dynamics, a remote response is elicited not just from forcing at different longitudes, but also from forcing at different latitudes.

Some of the previous work on latitudinally distant response has focused on the role of baroclinic Kelvin waves, which operate on timescales of months. For example, Kawase (1987) and Huang et al. (2000) studied the adjustment of the thermocline depth to the switch-on of a localized source of dense water using a reduced-gravity, shallow-water model. In these initial value problems, the steady state is reached through rapid propagation of Kelvin waves followed by a slower adjustment due to Rossby waves. In both Kawase (1987) and Huang et al. (2000) the sink of thermocline water associated with the high-latitude forcing is balanced by a distributed upward flux of mass provided by parameterized vertical mixing between the thermocline and the quiescent abyss. Although the *amplitude* of the thermocline depth anomaly is inversely proportional to the vertical mixing parameter, the *pattern* of circulation becomes independent of the mixing as long as the mixing timescale is longer than the Rossby wave transit time. This is the realistic limit. In this weakly diffusive regime, a steady response is obtained far away from the mass source: in the single basin calculation of Kawase

Corresponding author address: Paola Cessi, Scripps Institution of Oceanography, UCSD-0213, La Jolla, CA 92093-0213.
E-mail: pcessi@ucsd.edu

(1987) there is a steady circulation in the southern, unforced, hemisphere as well as in the northern one; in the global geometry considered by Huang et al. (2000) there is flow in every basin, although the source is confined to the North Atlantic.

While the steady state is well understood, at least in the context of a simple baroclinic model, the time-dependent global response of the upper ocean at low frequencies has received less attention, and this is the focus of the present work.

A notable exception is the work of Hsieh and Bryan (1996), who examined the response of the global upper ocean to constant heating localized in the high latitudes (either in the North Atlantic or in the Southern Ocean). In this case there is no mixing with the abyssal ocean that compensates the heating source so that the both the thickness of the thermocline and the global sea level increase in time. The sea level rise is not spatially uniform, and the instantaneous pattern obtained after 70 yr is qualitatively similar to the steady solution of Huang et al. (2000), especially insofar as the remote response is concerned. Both Hsieh and Bryan (1996) and Huang et al. (2000) find that the interior remote response is slow: because of the global scale of the adjustment even the directly forced subbasin responds on a multidecadal timescale; that is, adjustment of the directly forced region requires much longer than the local transit time of baroclinic Rossby waves.

The conclusion of Hsieh and Bryan (1996) and Huang et al. (2000) that there is a substantial remote response is at odds with the recent result of Johnson and Marshall (2002) that only a small fraction of the signal reaches beyond the forced hemisphere: our interpretation of this contradiction is that Johnson and Marshall (2002) are in a regime where the vertical mixing timescale is faster than the transit time of baroclinic Rossby waves.

In the present study, we examine the response to periodic forcing and inquire whether there is a preferred pattern and frequency that is especially effective at exciting a remote signal. This quest is motivated by recent results (Cessi and Primeau 2001; Cessi and Louazel 2001; Primeau 2002) showing that at decadal frequencies there are basin modes with characteristic frequencies: the timescale defined by the lowest eigenfrequency is an instrinsic property of the ocean. The dynamics of these large-scale basin modes involves only mass conservation and geostrophy. Because of their large scale, most of the modal energy is in the form of available potential energy so that the modal damping timescale is decadal even though the friction in the momentum equations corresponds to a few days. The hallmark of these basin modes is a synchronous oscillation of the eastern boundary pressure, which at low frequencies is uniform in space. The time-dependent eastern boundary pressure radiates a field of long Rossby waves that propagate westward. When the long Rossby waves reach the western wall, some of the energy is reflected into short eastward Rossby waves that are rapidly dissipated, but some energy excites a pressure signal on the boundary. At low frequencies, this boundary pressure is coherent all along the basin's perimeter, and thus transmits energy back to the eastern boundary, initiating more Rossby waves. As detailed in Primeau (2002), this low-frequency boundary pressure signal is not a free Kelvin wave since the latter is characterized by a boundary pressure that varies along the boundary, is associated with cyclonic propagation, and has a characteristic boundary trapping that scales as the deformation radius. None of these three signatures are present in low-frequency basin modes because at a decadal period the wavelength of a free baroclinic Kelvin wave would be of the order of 10^6 km, much larger than the circumference of the earth. Instead Primeau (2002) proves that the boundary signal is associated with low-frequency gravity waves forced by the interior Rossby waves.

We show in this paper that the boundary pressure feedback on the interior flow is the vehicle through which the interior circulation at one latitude induces flow in regions as remote as the opposite hemisphere, or even another basin connected through a circumpolar channel.

2. Model formulation

Our point of departure is the reduced-gravity shallow-water equations with friction and wind forcing. This is a minimal model for baroclinic flow in planetary basins since it also represents the evolution of the first baroclinic mode. The model excludes processes such as nonlinear coupling of different vertical modes. The strongest coupling affecting the first vertical mode is due to the wind-driven steady component of the second baroclinic mode (Dewar 1998; Liu 1999). However, this nonlinearity is weak so that properties of the first baroclinic mode are largely unchanged, and the reduced-gravity one layer is a surprisingly accurate approximation of the first baroclinic mode. It is also the case that most of the SSH perturbations, η, can be inferred from the thermocline displacement, h of the first baroclinic mode, through $\eta = -(g'/g)h$. Thus, remarkably, despite the exclusion of important processes such as production of baroclinic eddies, this simple formulation reproduces the low-frequency wind-driven pressure fluctuations observed in long time series (Sturges and Hong 2000). The resilience of baroclinic Rossby waves is confirmed by satellite observations of the interannual sea surface height (SSH) signal, which reveals a basinwide coherent pattern of Rossby waves in all oceans. The latter, although most prominent on the eastern side of the basins, survives westward all the way to the boundary current extension regions (Fu and Chelton 2001).

We consider a rectangular basin with $-L_y < y < L_y$ as the latitudinal coordinate and $0 < x < L_x$ as the cartesian longitudinal one, as shown in Fig. 1. In section

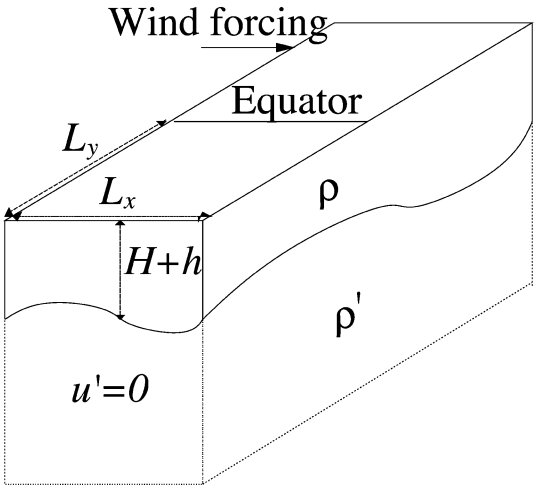

FIG. 1. A schematic figure of the basin geometry. The lower layer is at rest.

4, two basins connected at high latitudes by a periodic channel will be considered (cf. Fig. 8).

We parameterize the eddy fluxes through linear Rayleigh friction so that the oceanic flow is governed by the momentum equations:

$$u_t + uu_x + vu_y - fv = -g'h_x - ru + \frac{\tau}{\rho(H+h)}, \quad (1)$$

$$v_t + uv_x + vv_y + fu = -g'h_y - rv, \quad (2)$$

and the mass conservation equation:

$$h_t + [(H+h)u]_x + [(H+h)v]_y = 0. \quad (3)$$

In (1)–(3)

$f = \beta y$ is the Coriolis parameter,
u and v are the zonal and meridional velocities,
r is the coefficient of linear drag,
g' is the reduced gravity,
ρ is the mean density,
h is the interface displacement around the mean constant value H, and
τ is the zonal component of the wind stress.

Boundary conditions of no-normal flow are imposed on the solid walls, that is, $\mathbf{u} \cdot \mathbf{n} = 0$, so that total mass is conserved

$$\int_0^{L_x} dx \int_{-L_y}^{L_y} h\, dy = 0. \quad (4)$$

The integral constraint in (4) is obtained by integrating the mass conservation equation (3) over the domain and defining the mean layer thickness H as the initial average depth of the layer.

The simple geometries considered here omit the sphericity of the earth and the detailed crenellations of the coastline. As detailed in Cessi and Louazel (2001), the dominant dynamics at low frequency is that of long Rossby waves and the essential timescale is their transit time. On the sphere $\beta \propto \cos\phi$, where ϕ is the latitude, but $\cos\phi$ also appears as the metric term that converts longitude λ to distance x: $\Delta x = \Delta\lambda a \cos\phi$, where a is the spherical radius. Consequently there is a remarkable cancellation of the metric term when considering Δx divided by β. Thus the long Rossby wave transit time is identical in Cartesian and spherical geometry. As for the details of the coastline, Primeau (2002) has shown that they are irrelevant for the large-scale, low-frequency dynamics of baroclinic Rossby waves in a basin.

The low-frequency, weakly dissipated limit

Because we are concerned with forcing at periods decadal and longer, the equations can be simplified by neglecting the inertial terms. Moreover, for small-amplitude flows, the nonlinear terms can also be neglected, and the flow is in geostrophic balance except in thin frictional boundary layers. As detailed in Cessi and Louazel (2001), this implies that the interior dynamics is governed by combining the planetary geostrophic limit of (1) and (2) with the linearized mass conservation (3). Thus, for small friction, the interior solution satisfies

$$h_t - ch_x = \left(\frac{\tau}{f\rho}\right)_y, \quad (5)$$

$$c(y) \equiv \beta g' H/f^2, \quad (6)$$

where we have indicated with c the speed of long Rossby waves. The velocities are related to h by the diagnostic equations

$$-fv = -g'h_x + \frac{\tau}{\rho H}; \qquad fu = -g'h_y. \quad (7)$$

The single boundary condition admitted by (5), $u = 0$ at $x = L_x$, is satisfied by the condition on h

$$h = h_0(t) \quad \text{at } x = L_x. \quad (8)$$

Here $h_0(t)$ is an arbitrary function of time determined by the supplemental constraint of total mass conservation (4). The condition (4) can be applied to the interior solution in (5) because the frictional corrections modify h only in thin boundary layers, whose contribution to the mass integral is negligible.

An analysis of the equatorial boundary layer (omitted here) reveals that the condition (8) approximately applies even across the equator so that on decadal timescales the pressure is approximately independent of position all along the eastern boundary of the basin. Thus the interior dynamics that in Cessi and Louazel (2001) was confined to the extra-equatorial region extends across the equator into the other hemisphere. It is precisely the time-varying pressure on the eastern boundary that acts as a source of motion in latitudes that are not directly forced by the wind stress. In particular, if only the Northern Hemisphere is forced, then this boundary

signal freely crosses the equator and excites motion in the Southern Hemisphere.

3. Periodic forcing in a closed basin

In this section we specialize to forcing that is periodic in time and confined to a single hemisphere. The goal is to examine the response in the hemisphere that is not directly forced. Because the response to low-frequency, large-scale wind-driven forcing is well described by the linearized vorticity equation (5), the consideration of more complicated time dependence (i.e., stochastic process) can be achieved by linear superposition of the solutions at each frequency. Thus we consider a wind stress curl of the form

$$\left(\frac{\tau}{\rho f}\right)_y = \begin{cases} \mathrm{Re}[\Gamma(x, y)\, \exp(i\omega t)] & \text{if } y > 0, \\ 0 & \text{if } y \le 0, \end{cases} \tag{9}$$

so that Γ is the Fourier transform of the wind stress curl. Neglecting an initial transient, the response will also be of the form

$$h(x, y, t) = \mathrm{Re}[\hat{h}(x, y)\, \exp(i\omega t)]. \tag{10}$$

Substituting (10) into (5), we find that $\hat{h}$ is given by

$$\hat{h} = h_0 \exp\left[\frac{i\omega(x - L_x)}{c}\right] - c^{-1} \int_{L_z}^{x} \Gamma(\hat{x}, y) \exp\left[\frac{i\omega(x - \hat{x})}{c}\right] d\hat{x}. \tag{11}$$

The solution (11) satisfies the eastern boundary condition (8) and in the latitudinal bands where the forcing vanishes $\hat{h}(x, y)$ is entirely determined by the time-dependent variation on the eastern boundary, proportional to h_0. The latter constant is determined by enforcing mass conservation (4), which results in

$$h_0 = D^{-1} \int_0^1 d\tilde{x} \int_{-1}^1 \Gamma(\tilde{x}, \tilde{y})(e^{-i\tilde{\omega}\tilde{x}\tilde{y}^2} - 1)\, d\tilde{y}, \tag{12}$$

$$D \equiv \frac{g'H}{\beta L_x L_y^2} \int_{-1}^1 \tilde{y}^{-2}(1 - e^{-i\tilde{\omega}\tilde{y}^2})\, d\tilde{y}. \tag{13}$$

We have defined the nondimensional frequency and spatial coordinates

$$\tilde{\omega} \equiv \omega \frac{\beta L_x L_y^2}{g'H}, \qquad (\tilde{x}, \tilde{y}) = \left(\frac{x}{L_x}, \frac{y}{L_y}\right), \tag{14}$$

in order to highlight the dependence of h_0 on the nondimensional frequency, $\tilde{\omega}$. Notice that the relevant timescale in the problem is the transit time of long Rossby waves at the high-latitude boundary:

$$T_{\mathrm{RW}} \equiv L_x/c(L_y) = \beta L_x L_y^2/(g'H). \tag{15}$$

The expression for the eastern boundary displacement (12) demonstrates that all latitudes are coupled in contrast with the usual interpretation that, in the long wave approximation, the dynamics of Rossby waves at each latitude are independent (e.g., Frankignoul et al. 1997).

The denominator, D in (13), vanishes only for $\tilde{\omega}$ complex. The zeroes of D approximate the discrete low-frequency eigenvalues of the linear homogeneous equation associated with (1)–(3) in the limit of small friction. In particular, the least damped basin mode straddles both hemispheres. Its interior spatial structure is

$$\hat{h} = h_0 \exp[i\omega(x - L_x)/c], \tag{16}$$

with ω given by the smallest zero of D (i.e., the zero closest to the origin in the complex ω plane). Because c becomes infinite at the equator, the pressure along the equator equals that on the eastern boundary, and the depth anomaly is symmetric about the equator. As an example, the least damped eigenmode obtained by finding numerically the zeroes of D in (13) for the parameter values in (25) is

$$\tilde{\omega}_{\mathrm{eig}} = 7.54 + 1.70i, \tag{17}$$

corresponding to a period of 16.4 yr and an e-folding decay time of 11.6 yr. The essential point is that adjustment to steady state is achieved in a time that must exceed the longest eigenperiod.

The large-scale approximation (16) compares well to the least-damped eigenmode obtained solving the unforced, linearized shallow-water equation associated with the system (1) through (3), assuming a time dependence of the form (10), as illustrated in Fig. 2. Notice that in the shallow water system the depth is indeed symmetric around the equator, it is approximately constant on the eastern boundary and equal to the value at the equator, as predicted by the interior approximation (16).

For ω real, the denominator D does not vanish and it is a measure of the mass flux across the equator because the storage rate in the Southern Hemisphere is given by

$$\int_0^{L_x} dx \int_{-L_y}^0 h_t\, dy = \mathrm{Re}[h_0 D \exp(i\omega t)] L_x L_y/2. \tag{18}$$

At least for the simple geometry considered here, (12) shows that the mass flux across the equator depends on the frequency and shape of the wind stress curl over the whole hemisphere.

a. Optimal forcing: An upper bound on the remote response

Given that the least damped basin mode is interhemispherical, it is expected that forcing localized in one hemisphere can excite a distant response. However, because the damping of the basin modes is not weak, it is not clear what forcing frequency would optimally excite a remote response. In this section we address this question and determine both the spatial pattern and the frequency of the forcing that give rise to the largest

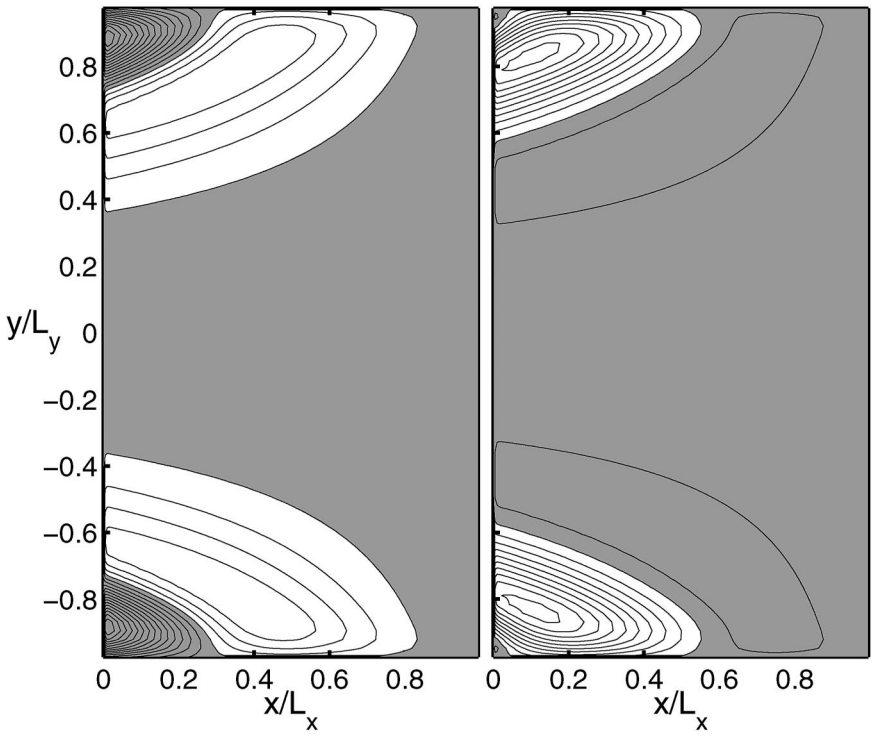

FIG. 2. The (left) real and (right) imaginary part of the height field, $\hat{h}(x, y)$, for the least damped eigenmode of the linearized, unforced system associated with (1)–(3). All the parameters are as in (25), and the friction is $r = 5.7 \times 10^{-7}$ s^{-1}. The eigenvalue is $\omega = (1.15 + i0.78) \times 10^{-8}$ s^{-1}, corresponding to a period of 17.3 yr and an e-folding decay time of 4 yr. The amplitude of the eigenmode is arbitrary and negative values are shaded.

response in the hemisphere that is not directly forced, subject to a constraint on its norm.

From (11), the response in the unforced region is given by

$$h_{\text{remote}} = \text{Re}\{h_0 \exp[i\omega(x - L_x)/c + i\omega t]\}. \quad (19)$$

This is a long Rossby wave emanating synchronously from the eastern boundary and with crests and troughs arriving at the western wall at times that increase with the square of the latitude.

As a measure of the response in the unforced hemisphere we use the average of h^2_{remote} over one period of the oscillation, which coincides with $|h_0|^2/2$, and is independent of x and y. This measure is proportional to the potential energy in the unforced hemisphere, which is the dominant form of energy in the long-scale limit. The maximization of the energy is subject to a constraint on the norm of the forcing, namely

$$\int_0^1 d\tilde{x} \int_{-1}^1 \Gamma\Gamma^* \, d\tilde{y} = \text{const.} \quad (20)$$

The optimization is obtained by maximizing the functional $\mathcal{F}(\Gamma, \Gamma^*)$, defined as

$$\mathcal{F} \equiv h_0 h_0^* + \lambda\left(\int_0^1 d\tilde{x} \int_{-1}^1 \Gamma\Gamma^* \, d\tilde{y} - \text{const}\right), \quad (21)$$

where λ is a Lagrange multiplier. Given the expression (12) for h_0 as a function of Γ, we find that the variation of $\mathcal{F}$ with respect to Γ^*, for ω fixed, is

$$\delta\mathcal{F}|_{\delta\Gamma^*} = h_0 D^{-1} \int_0^1 d\tilde{x} \int_{-1}^1 (e^{i\tilde{\omega}\tilde{x}\tilde{y}^2} - 1)\delta\Gamma^* \, d\tilde{y} + \lambda \int_0^1 d\tilde{x} \int_{-1}^1 \Gamma\delta\Gamma^* \, d\tilde{y}. \quad (22)$$

For a maximum, $\delta\mathcal{F}$ (and its complex conjugate) must vanish for an arbitrary variation of $\delta\Gamma^*$ (and $\delta\Gamma$), and so

$$\lambda\Gamma = h_0 D^{-1}(1 - e^{i\tilde{\omega}\tilde{x}\tilde{y}^2}). \quad (23)$$

The optimal wind stress curl has a component that is constant in space and a component that is a pattern of waves propagating at the local Rossby wave speed, similar to the eigenmodes of the systems, (16). While the free basin modes are constant at the eastern boundary, there the optimal wind stress curl varies the most while vanishing at the western boundary. Because the free modes are Rossby waves generated at the eastern wall by the boundary pressure, the most efficient way to excite them is to maximize the Ekman pumping at the eastern boundary and then force each free wave coherently by propagating the wind stress curl at the same

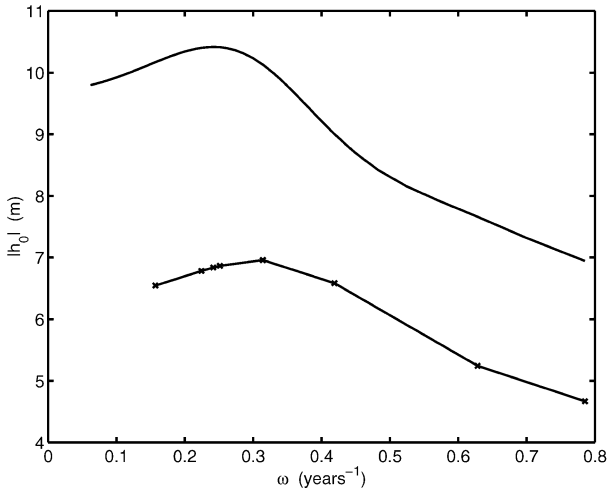

FIG. 3. The eastern boundary depth $|h_0|$ predicted by the interior approximation (12) (smooth solid curve) as a function of the frequency ω of the optimal forcing (24). The x marks show the time- and space-averaged $\sqrt{2\langle h\rangle^2}$ in the unforced hemisphere obtained by numerically integrating the nonlinear shallow-water equations with friction, $r = 8 \times 10^{-7}$ s^{-1}, for the same forcing.

speed. The pattern of optimal forcing is not realistic, but it provides an upper bound on the amplitude of *any* ocean remote response to atmospheric forcing subject to the normalization (20).

Comparing (18) with (12) shows that a wind stress curl of the shape (23) also maximizes the flux of mass across the equator.

The Lagrange multiplier λ is determined by the condition (20). Because the spatial structure of the optimal forcing depends on ω, the normalization condition requires the amplitude of the forcing to depend on the frequency. The final expression for the optimal forcing as a function of the spatial coordinates and of the frequency is thus

$$\Gamma(\tilde{x}, \tilde{y}) = \frac{\tau_0}{\rho\beta L_y^2\sqrt{2}}\left[1 - \int_0^1 \frac{\sin(\tilde{\omega}s^2)}{\tilde{\omega}s^2}\, ds\right]^{-1/2} \times (1 - e^{i\tilde{\omega}\tilde{x}\tilde{y}^2}). \quad (24)$$

In the following we choose $\tau_0 = 0.1$ N m^{-2}. For this and subsequent calculations we use the following values:

$$\beta = 2.3 \times 10^{-11}\ \text{m}^{-1}\ \text{s}^{-1}, \qquad H = 500\ \text{m},$$
$$g' = 0.02\ \text{m s}^{-1} \qquad L_x = 7.5 \times 10^6\ \text{m},$$
$$L_y = 6 \times 10^6\ \text{m}. \quad (25)$$

With this choice, the area of the basin is $2L_yL_x = 9 \times 10^{13}$ m^2, which is 60% of the surface area of the Pacific Ocean. The β term is evaluated at the equator, and the mean depth and stratification are chosen to be typical of the subtropical thermocline in the Pacific.

Figure 3 shows the eastern boundary depth, $|h_0|$, as a function of frequency for the optimal forcing (24). The offset between the curves in Fig. 3 is because the theoretical result (12) is based only on interior dynamics and does not account for the frictional boundary layers. Specifically, the northern boundary layer contains a substantial amount of mass.

The forcing frequency $\tilde{\omega}$ is a parameter in the optimal forcing (24). Thus we can now maximize the optimal response by varying $\tilde{\omega}$. We find that the largest response is at $\tilde{\omega} = 4.9$. For the values quoted in (25) this corresponds to a period of 26 yr. Thus the optimal forcing is peaked at a period that is quite different from that of the least damped eigenmode: this is typical of non-normal systems such as (1) through (3) (Farrell and Ioannou 1996).

Figure 4 (left panel) shows a snapshot of the solution (11) for the optimal wind forcing (24). Also shown (right panel) is h obtained by numerically integrating the reduced-gravity shallow-water equations (1)–(3) including friction and nonlinearity. Because the optimal forcing (24) has its maximum along the northern boundary, where the analytic approximation must be corrected in a frictional boundary layer, the response of the full shallow-water system is smaller than that predicted by the inviscid approximation. In all the numerical calculations that we use the following value for the frictional parameter, which guarantees an adequate resolution of the western boundary layer:

$$r = 8 \times 10^{-7}\ \text{s}^{-1}, \quad (26)$$

corresponding to a decay time of 14.4 days. An important point is that, even though the Ekman spindown timescale is about 14 days, the basin-scale oscillations damp only on several decades. Physically this is because only a fraction $(R/L)^2 \ll 1$ of the oscillation energy is kinetic energy (R is the baroclinic deformation radius, $\sqrt{g'H}/f$, and L the basin length scale). The largest discrepancies between the large-scale interior approximation and the shallow-water solutions are due to boundary layer corrections along the northern and southern walls, whose widths are of order $O(\sqrt{rL_x/\beta}) \approx 440$ km. This is illustrated in Fig. 5 where a snapshot of the zonally averaged interface displacement predicted by (11) (dashed line) is compared to that obtained from the numerical solution (solid line). The overestimate by the analytic approximation to h in the northern and southern boundary layers is compensated in the interior by an anomaly of the opposite sign (recall that the area under each curve must integrate to zero due to mass conservation).

The analytic approximations (12) and (24) also predict the dependence of the response on the optimal forcing's frequency. In Fig. 3, we show $\sqrt{2\langle h^2\rangle}$ (**x** marks), that is, the average over a period and over the unforced hemisphere of the rms interface displacement obtained from the numerical solution of (1)–(3). The wind stress is the optimal forcing (23) for different frequencies. Despite the disagreement in the frictional boundary layers the optimal response is obtained at approximately

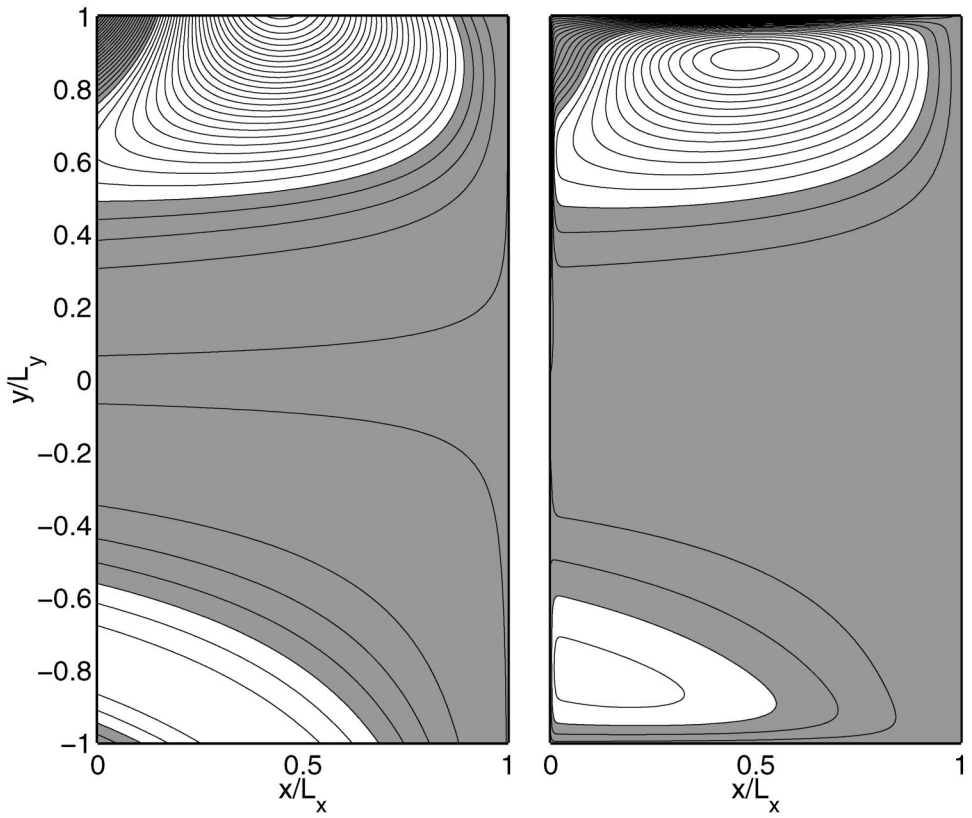

FIG. 4. (left) A snapshot of the analytic approximation to h for the optimal forcing (24) oscillating with a period of 26 yr. The maximum value of the wind is 0.085 N m^{-2}. The range in the Northern Hemisphere is from 80 to −67 m, while in the Southern Hemisphere it is −10 to 10 m. (right) The solution of h obtained solving (1)–(3) numerically at the same time. The range in the Northern Hemisphere is from 46 to −43 m, while in the Southern Hemisphere it is 6.0 to −6.7 m. The contour level is 3 m and negative contours are shaded.

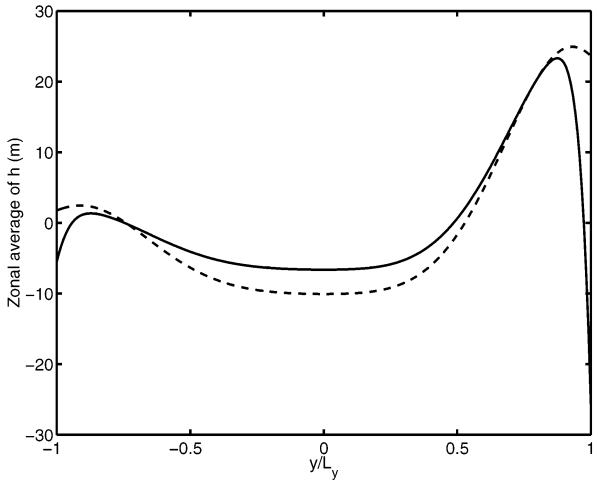

FIG. 5. The zonally averaged interface displacement shown in the right panel of Fig. 4 (solid line) is compared with the zonal average of h from the left panel of Fig. 4 (dashed line).

the same period (between 20 and 26 yr) as the analytical prediction.

Figure 6 shows four snapshots of h in the unforced hemisphere during half a period to illustrate the southwestward propagation of the remote response. Notice that the maximum displacement migrates from the equator and the eastern boundary toward the pole and the western wall during one period, so all of the Southern Hemisphere experiences a remote response. In both the analytic approximation and the shallow-water solution with small dissipation the remote thermocline displacement is approximately 15% of the locally forced depth variation. Notice that, although the optimal forcing excites a response in the shape of the least damped eigenmode, its pattern is nothing like it.

b. Suboptimal forcing

Because of the peculiar propagating structure of the optimal forcing, we enquire whether a substantial remote response is also elicited with a more generic shape of the wind stress. We thus explore the following family of wind stress patterns:

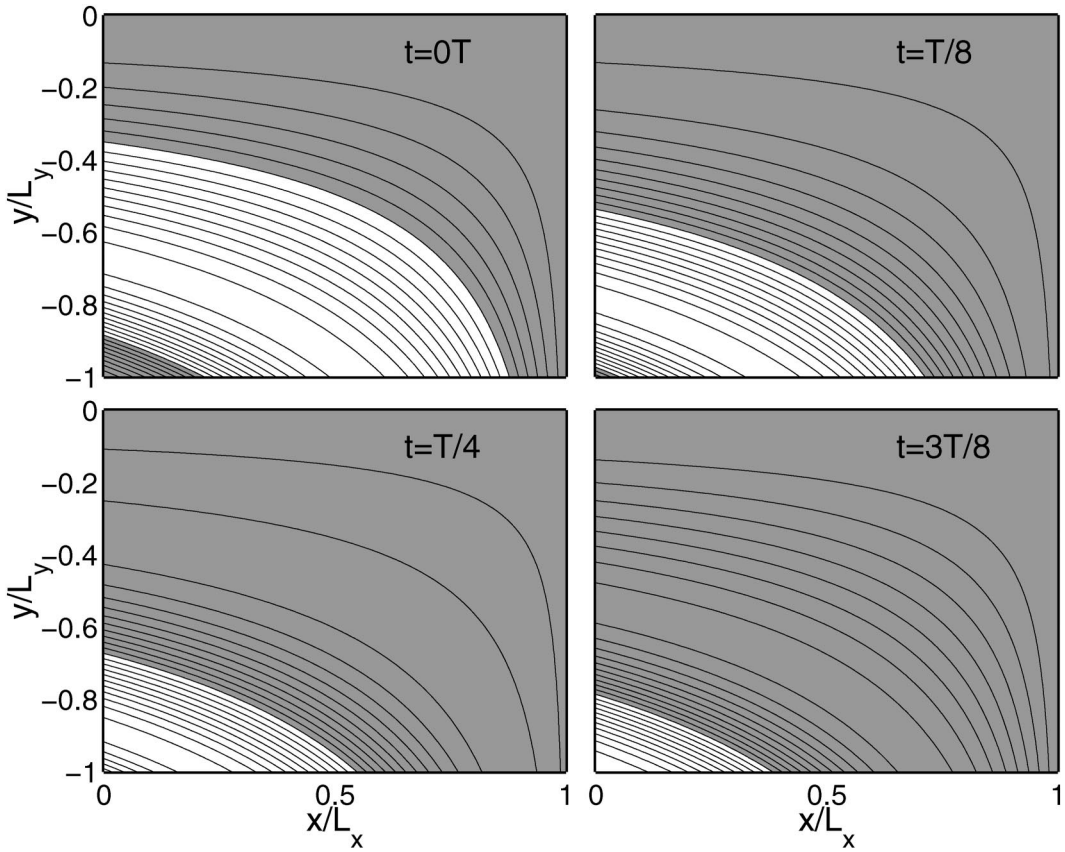

FIG. 6. Four snapshots of the analytic approximation to h in the Southern Hemisphere during 0.5 period for the optimal forcing (24), oscillating with a period of 26 yr. Notice that the maximum and minimum propagate poleward and westward. The contour level is 1 m and negative contours are shaded.

$$\tau = \tau_0 \exp[-(y - y_0)^4/l^4] \cos(\omega t), \qquad (27)$$

where both the central latitude y_0 and the scale l can be varied. This pattern of wind stress is standing, while that considered in the previous section is propagating. The hyper–Gaussian profile in (27) ensures that the forcing is localized in a strip $y_0 - l < y < y_0 + l$. This strip might, for instance, correspond to a storm track. At any rate, the localized standing waves pattern (27) is very different from the broad traveling pattern in (24), thus providing an assessment of the robustness of conclusions based on the optimal shape (24).

For the range of y_0 and l such that the hyper–Gaussian forcing is localized in the Northern Hemisphere, the maximum response in the Southern Hemisphere, subject to the constraint (20), is obtained when the central latitude of the forcing is $y_0 = L_y/2$, and its width is $l = 0.3L_y$. In order for (27) to have the same norm as (24) the amplitude of the wind stress in (27) must be $\tau_0 = 0.015$ N m^{-2}, which is much smaller than the wind stress amplitude of the optimal forcing. An analysis of the remote response, $|h_0|^2$, as a function of frequency reveals that the largest response is obtained at a period of 22 yr, rather close to the period of the optimal forcing (26 yr). However, the amplitude is smaller by about a factor of 3 than that produced by the optimal forcing (24), indicating that the efficiency of the optimization procedure considered in the previous section is high when the norm of the wind stress curl is kept fixed as in (20).

Figure 7 (left panel) shows a snapshot of the solution (11) for the wind stress (27), with $\omega = 2\pi/22$ yr. Also shown (right panel) is h obtained by numerically integrating the reduced-gravity shallow-water equations. The agreement between the theoretical prediction based on interior dynamics and the numerical solution with small friction is much better than that obtained with the optimal forcing because the response to a hyper-Gaussian forcing does not entail a northern boundary layer. Consequently, there is no ''missing-mass'' error. The agreement between the analytic inviscid approximation and the numerical solution with friction is good, not just as far as the amplitude of the response, but also as far as the optimal frequency is concerned. A series of numerical calculation, not shown here, varying the frequency of the wind stress, confirms that the largest response is indeed obtained when the period is 22 yr. Although the maximum remote response obtained with the family (27) is smaller than with the optimal forcing,

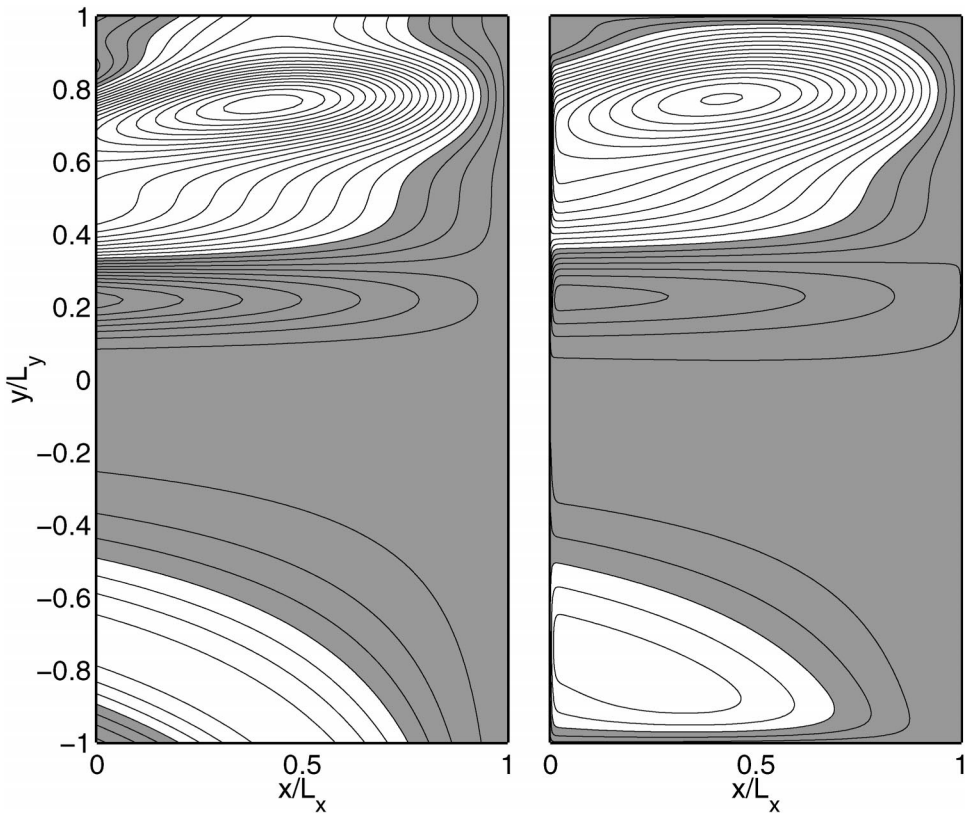

FIG. 7. (left) A snapshot of the analytic approximation to h for the hyper-Gaussian forcing (27), oscillating with a period of 22 yr. The range in the Northern Hemisphere is from 18 to −11 m, while in the Southern Hemisphere it is 3.6 to −3.5 m. (right) The interface displacement, h, obtained solving (1)–(3) numerically. The range in the Northern Hemisphere is from 15 to −7 m, while in the Southern Hemisphere it is 2.7 to −3.0 m. The contour level is 1 m and negative contours are shaded. For both the large-scale approximation (left) and the full shallow-water solution (right) the ratio of the remote to the locally forced response is about 25%.

the ratio of the displacement amplitude in the unforced to that in the forced region is larger with the suboptimal forcing in (27).

For both wind stress patterns considered in this section, there is an appreciable response in the unforced Southern Hemisphere. The remote response is maximum when the period is about 26 yr. In the following we assess the robustness of the solution to the geometry of the basin.

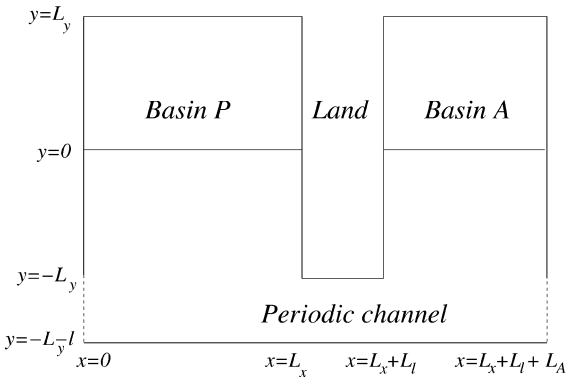

FIG. 8. The geometry of two basins with a circumpolar connection at the southern edge.

4. Two basins with a circumpolar connection

In this section we examine the coupled problem of two basins connected by a periodic channel at the southernmost edge. With reference to Fig. 8, the region $-L_y - l < y < -L_y$ is occupied by a reentrant channel that connects two basins of equal latitudinal extent, one of zonal width L_x and the other of zonal width L_A. The two basins are separated by a landmass of width L_l and by an infinitesimally thin solid boundary. In the following we will focus on a configuration with

$$L_x = 10.56 \times 10^6 \text{ m}, \qquad L_y = 6.6 \times 10^6 \text{ m}$$

$$L_A = L_x/2, \quad L_l = L_x/4, \quad l = 0.16L_y \tag{28}$$

so that the area of the basin P, of the basin A, and of the channel approximate those of the Pacific, of the Atlantic, and of the Southern Ocean, respectively.

The interior dynamics (5) still holds away from the

boundaries and in each enclosed basin the pressure on the eastern boundary is a function of time only. In the channel the periodicity condition $h(x, y, t) = h(x + L_x + L_l + L_A, y, t)$ applies.

In the following we will consider forcing that is periodic in time and confined to the Northern Hemisphere of basin P so that the Southern Hemisphere of P, the channel, and basin A are all unforced. Using the notation of section 3, the solution in basin P is given by

$$h_P = \mathrm{Re}[\hat{h}(x, y)\exp(i\omega t)],$$

$$\hat{h}(x, y) = h_0 \exp\left[\frac{i\omega(x - L_x)}{c}\right] - c^{-1}\int_{L_x}^{x} \Gamma(\hat{x}, y)\exp\left[\frac{i\omega(x - \hat{x})}{c}\right] d\hat{x}, \quad (29)$$

where h_0 is a constant, characterizing the amplitude of the oscillating depth at $x = L_x$.

Since basin A is unforced, the solution there is given by

$$h_A = \mathrm{Re}\{h_1 \exp[i\omega(x - L_x - L_l - L_A + ct)/c\}, \quad (30)$$

where h_1 is the amplitude of the oscillating depth at the eastern boundary of basin A.

The constants h_0 and h_1 are determined by enforcing mass conservation in each basin, or alternatively mass conservation in one basin and globally, as detailed shortly. Because the constraint of global mass conservation leads to consideration of the total mass in the periodic channel, we only need to examine the area average of h there.

Neglecting friction, the evolution equation for the zonally averaged depth $\overline{h}$ in the channel is

$$i\omega\overline{h} = 0, \quad (31)$$

so, in the absence of local forcing, the circumpolar region does not contribute to the mass displacement, and only the two basins need to be considered. The approximate result (31) does not imply that the channel is at rest: free Rossby waves propagate through the channel, but they have zero zonal average and do not contribute to mass storage.

The mass budget in basin A is

$$\int_{\mathrm{Area(A)}} h_t\, dx\, dy = H\int_{L_x+L_l}^{L_x+L_l+L_A} v|_{y=-L_y}\, dx, \quad (32)$$

stating that the total storage rate is balanced by the mass flux at the boundary between the basin and the channel.

The meridional velocity is in geostrophic balance even in the western boundary current so that

$$H\int_{L_x+L_l}^{L_x+L_l+L_A} v|_{y=-L_y}\, dx = \frac{g'H}{f|_{y=-L_y}}[h(L_x + L_l + L_A, -L_y, t) - h(L_x + L_l, -L_y, t)]. \quad (33)$$

The depth on the eastern boundary of basin A is independent of y and is obtained from (30). The depth on the southwest corner of basin A is within a western boundary layer and cannot be obtained from the interior approximation (30). However, the requirement that the geostrophic velocity normal to the southern edge of the landmass vanishes[1] leads to constant pressure on that boundary. Thus, the depth at the southwest corner of basin A equals h at the southeast corner of basin P, which in turn is the depth all along the eastern boundary $x = L_x$. We thus have

$$h(L_x + L_l, -L_y, t) = h(L_x, t) \quad (34)$$

so that the leading-order depth is constant all along the western and southern boundary of the landmass.

Substituting (29), (30), and (34) into (32) we find that

$$h_0 = h_1 S(\tilde{\omega}), \quad (35)$$

$$S(\tilde{\omega}) \equiv 1 + i\tilde{\omega}\int_{-1}^{1} d\tilde{y}\int_{0}^{L_A/L_x} \exp\left[i\tilde{\omega}\left(\tilde{x} - \frac{L_A}{L_x}\right)\tilde{y}^2\right] d\tilde{x}, \quad (36)$$

where the nondimensional frequency and coordinates defined in (14) have been used. To summarize, the mass budget in basin A, together with geostrophy and the condition of no flow through the southern boundary of the landmass, provides the connection (35) between the eastern boundary pressures of the two basins. Remarkably, the width of the landmass does not matter as long as there is no forcing at its southern tip.

The requirement that the area integrals of (29) and (30) add up to zero, so as to conserve total mass, leads to the following condition on h_0, analogous to (12):

$$h_0 = D'^{-1}\int_0^1 d\tilde{x}\int_{-1}^{1} \Gamma(\tilde{x}, \tilde{y})(e^{-i\tilde{\omega}\tilde{x}\tilde{y}^2} - 1)\, d\tilde{y}, \quad (37)$$

$$D' \equiv \frac{g'H}{\beta L_x L_y^2}\left[1 - S(\tilde{\omega})^{-1} + \int_{-1}^{1} \tilde{y}^{-2}(1 - e^{-i\tilde{\omega}\tilde{y}^2})\, d\tilde{y}\right]. \quad (38)$$

Notice that neither the width of the continent nor the size of the channel enter the expression for h_0 because these subdomains do not contribute to the global mass balance. The eastern boundary pressure here differs from that in the closed basin of section 3 only through denominators D and D' [cf. (13) and (38)]. The two denominators become identical when the width of basin A vanishes, and so the results of section 3 apply also to a semienclosed basin whose southern solid boundary is replaced by a reentrant channel.

Analogous to (18), the denominator D' is proportional

[1] As discussed in CL01, the thickness of the frictional boundary layer on a southern boundary is $O(\sqrt{rL_x/\beta})$, leading to negligible correction on the geostrophically balanced depth.

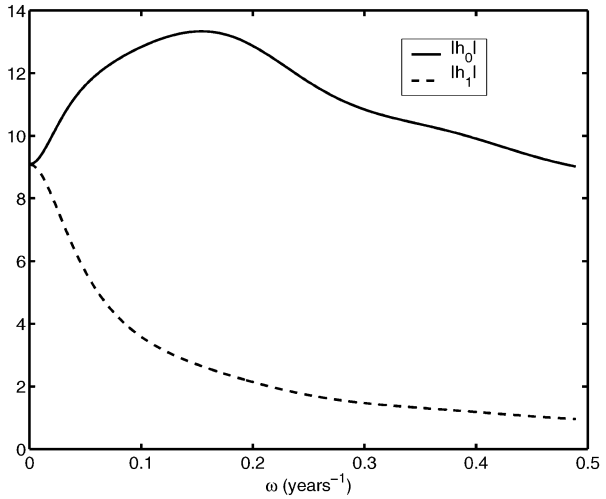

FIG. 9. The eastern boundary depth in basin P, $|h_0|$, and the eastern boundary depth in basin A, $|h_1|$, (both in meters) predicted by the interior approximations (29) and (30) as a function of the dimensional frequency, ω, of the optimal forcing (24).

to the total mass flux across the equator for the two basins combined. A simple calculation shows that the storage rate of the combined Southern Hemispheres is given by

$$\int_0^{L_x+L_I+L_A} dx \int_{-L_y}^{0} h_t \, dy = \mathrm{Re}[h_0 D' \exp(i\omega t)] L_x L_y/2. \quad (39)$$

Because the expressions for h_0 in (12) and (37) only differ through the denominators D and D', the spatial structure of the forcing (24) optimally excites the response also when considering several interconnected basins.

Figure 9 shows the amplitudes of the two eastern boundary pressures for basin P (solid line) and basin A (dashed line), as a function of the forcing frequency. For the value of parameters in (28), the Southern Hemisphere of basin P is maximally excited at a period of 45 yr. This period is longer that the optimal value found in section 3 because L_x and L_y are larger in the present example [cf. (28) with (25)]. In fact, the optimal nondimensional frequency for $|h_0|$ is $\tilde{\omega} = 5.2$, which is slightly *higher* than that obtained with a single basin in section 3 ($\tilde{\omega} = 4.9$). The essential point is that the optimal forcing period is comparable to the transit time of baroclinic Rossby waves in the subpolar region of the forced basin, both in a single basin and in two basins (and presumably also three basins) connected by a periodic high-latitude channel.

The response in basin A increases with increasing period and becomes equal to that of basin P in steady state when the pressure difference between the eastern and western boundary vanishes, and so no net flux of mass enters or leaves each basin. Of course, when the frequency is very close to zero, the approximation (29) is no longer valid because the neglected frictional effects become essential.

As an example, we show in Fig. 10 a snapshot of h forced by a wind stress curl given by (24) oscillating at a period of 40 yr for the geometry of Fig. 8. The solution is obtained by solving the shallow water system (1)–(3) with the parameters in (28) and $r = 8 \times 10^{-7}$. A comparison with the solution obtained in the closed basin, whose forcing oscillates at 26 yr (cf. Figs. 4 and 10), shows that the spatial pattern of the response in the Southern Hemisphere of the forced basin is very similar in the two cases, confirming the interpretation that a proper mode of the system is excited. The response in basin A is 15% of the response in the Southern Hemisphere of basin P and it is symmetric around the equator, as predicted by the interior approximation.

To quantify the role of each subasin in the global mass balance, we plot in Fig. 11 the volume anomaly stored in the various regions of the domain as a function of time. The storage rate is proportional to the flux of mass across the open portion of each subregion and can be approximately obtained by multiplying the storage by the frequency ω (and shifting the time series by one quarter period). The largest storages are in the Northern and Southern Hemispheres of the forced basin, P. For the values used here they imply a flux of mass across the equator which peaks at 1.7 Sv (Sv $\equiv 10^6$ m^3 s^{-1}). Because the storages in the two hemispheres of basin P do not cancel, there is a flux of mass at the boundary between basin P and the channel that peaks at 0.4 Sv in the example of Fig. 11. The storage in the periodic channel is negligible, and so all the mass leaving basin P is fluxed into basin A, whose storage is equally partitioned between the two hemispheres. In basin A, the mass flux across the equator peaks at 0.2 Sv, about 12% of the corresponding maximum flux in basin P.

5. Summary and discussion

We have examined the remote response to time-dependent wind forcing confined to a single hemisphere in domains of simplified geometry. A time-dependent flow is obtained in unforced regions through the Rossby waves that radiate from the eastern boundary. The eastern boundary pressure fluctuates in time so as to guarantee that the mass of the active layer is conserved. Combining this with simple dynamics leads to analytic results that enable us to survey the parameter space and to identify the controlling nondimensional factors.

In the absence of alongshore winds, the fluctuations are synchronous all along the eastern coasts on the decadal timescales considered here. Unlike Kelvin waves, these disturbances are robust to coastline irregularities (Primeau 2002).

We find that for a closed basin the remote response in the unforced hemisphere is maximally excited by winds oscillating at a period longer than, but of the same

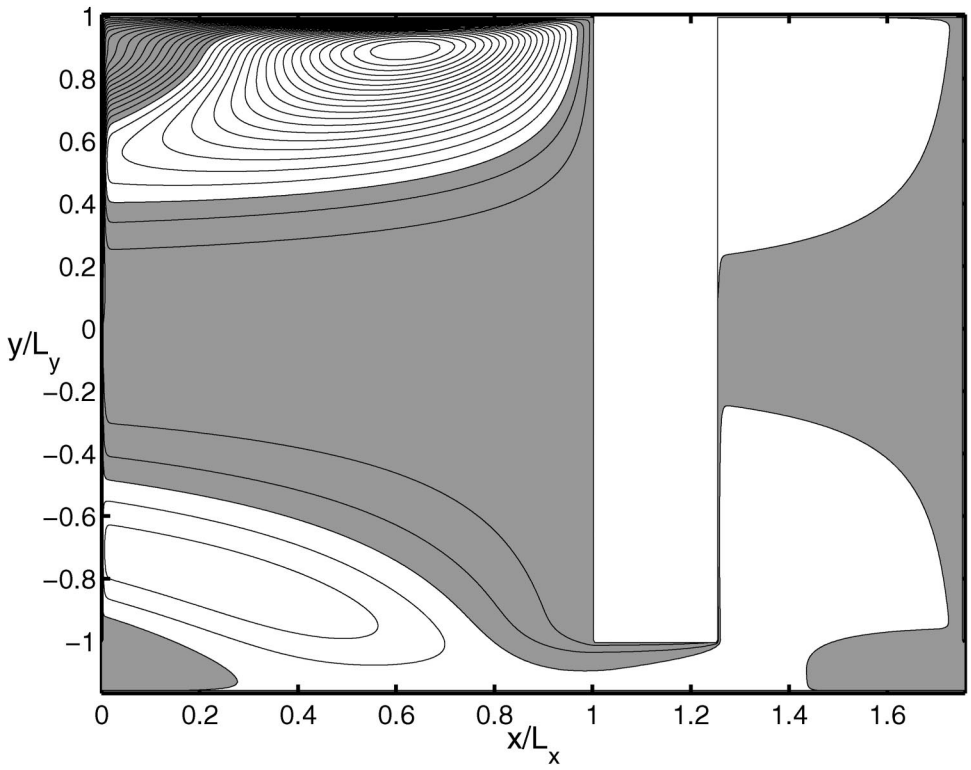

FIG. 10. A snapshot of the interface displacement, h, obtained solving (1)–(3) numerically in the geometry shown in Fig. 8. The wind stress is obtained from the optimal forcing (24), oscillating with a period of 40 yr. The maximum wind-stress is 0.053 N m^{-2}. The range in basin P is from -41 to 39 m in the Northern Hemisphere and from -5 to 6 m in the Southern Hemisphere. In basin A the range is -1 to 4 m. The contour level is 2 m and negative contours are shaded.

order as, the period of the least damped eigenmode of the system. This eigenmode is characterized by depth anomalies that are maximum in the poleward-west corner of the basin and minimum on the eastern boundary and the equator and have a period roughly equal to T_{RW} in (15). The pressure on the equator for these basin modes equals that along the eastern boundary, suggesting that the low-frequency oceanic variability generated in high latitude can influence tropical dynamics without any atmospheric mediation.

For basins that are symmetric around the equator the low-frequency basin modes have no net mass flux across the equator. However, when periodic wind forcing is applied to a single hemisphere, the storage rate in that hemisphere does not vanish, and there is a time-dependent mass flux passing across the hemispheres, even if the local forcing vanishes there. Replacing the southern boundary with a reentrant channel connecting the high-latitude edge of the unforced hemisphere leaves the solution unchanged.

When two basins connected at the southern boundary by a periodic channel are considered, forcing in the Northern Hemisphere of one basin induces a time-dependent response in the other basin. This oceanic teleconnection is characterized by a mass flux across the boundary between the forced basin and the channel. The channel stores a negligible amount of mass, instead acting as a conduit between the two basins whose storages are out of phase. The essential point is that, on these long timescales, mass balance is not achieved within one basin, but globally and with negligible contribution from the reentrant portion.

The lack of signal in the channel when the forcing is in the Northern Hemisphere is in agreement with the finding by Hsieh and Bryan (1996) of a weak Southern Ocean sea level rise in response to heating in the Arctic. In contrast, Huang et al. (2000) find a sizeable signal in the Antarctic Circumpolar Current region sustained by a balance between lateral eddy exchanges and vertical upwelling due to mixing (both parameterized). The latter process is absent in both Hsieh and Bryan (1996) and in our model, and it obviously has a qualitative repercussion in reentrant geometries.

We have considered wind stresses whose amplitude ranges from 0.01 to 0.05 N m^{-2} oscillating over several decades: the upper range of values is larger by about a factor of 2 from those reported by Roemmich et al. (2001) on interannual scales. With such wind stresses, the remote response of the interface displacement is of the order of several meters. For the choice of parameters (25), a thermocline depression h of 10 m is associated with a sea level change, $\eta = -(g'/g)h$, of 2 cm, which

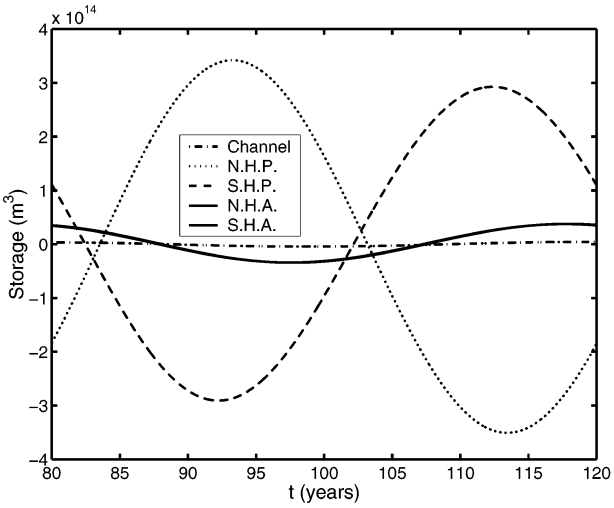

FIG. 11. The mass storage in each subregion is plotted as a function of time for the calculation shown in Fig. 10. Notice that the storage is equipartitioned between the two hemispheres in basin A, and so the two solid lines almost coincide. The storage rate in meters cubed per second can be obtained by multiplying the storages by $\omega = 5 \times 10^{-9}$ s^{-1}.

is of the same order as the decadal trend currently observed (Douglas 2000), indicating that sea level changes observed at one location might be generated by very distant forcing.

Within the confines of a highly idealized geometry, we have performed a calculation with two basins having an area comparable to that of the surface Pacific and Atlantic, respectively. We obtain a mass flux on multidecadal timescales across the equator of the model Pacific that is of magnitude comparable to that measured by Roemmich et al. (2001) at 24°N using geostrophic flow above 800 m. The observed geostrophic flow in the thermocline is somewhat compensated by Ekman transport, but presumably the compensation decreases on longer timescales.

Besides the hemisphere-integrated transport fluxes, our calculation shows that the low-frequency global thermocline displacement obtained from localized forcing has a nontrivial large-scale pattern that reflects the dynamics of baroclinic Rossby waves coupled through the pressure along the solid boundaries. Regardless of the shape of the forcing and the basin geometry, the interface displacements within the semienclosed basins all share a minimum in response in the eastern tropical region and a gyrelike pattern in both hemispheres at midlatitudes (cf. Figs. 4, 7, and 10). These patterns are very similar to those found in the steady-state calculations of Huang et al. (2000) and in the initial value problem of Hsieh and Bryan (1996). A similar pattern in transient sea level rise is found by Bryan (1996) in a calculation using the Geophysical Fluid Dynamics Laboratory coupled model with enhanced greenhouse warming, about 45 years after the warming starts.

Our analytic approximation clarifies that the pressure on the boundaries is the vehicle for communication between basins and that Rossby waves transmit the information to the interior. We also hope to dispell the commonly received opinion that free Kelvin waves are an essential element in the low-frequency oceanic fluctuations: there are no free Kelvin waves at decadal periods that can fit in any terrestrial basin. Instead the field of Rossby waves forces low-frequency, large-scale gravity waves that redistribute the mass coherently within the global ocean. Because of the large-scale nature of the motions involved, the details of the coastline are irrelevant.

Here, we have limited our study to a single vertical baroclinic mode, or equivalently to one reduced-gravity layer. The inclusion of several vertical modes (or layers) would allow for more complex processes, for example, the interaction with time-mean currents and the spontaneous generation of time-dependent flows. Although advection by mean currents is bound to be important, we are very encouraged by some recent results by D. Stammer et al. (2003, unpublished manuscript: concerns the response of the global ocean to radiative forcing anomalies over Asia) showing very similar propagating patterns of remote SSH anomalies in the Atlantic and Pacific in response to anomalies of heat and wind stress forcing confined to the Indian Ocean in a multiyear calculation using the Massachusetts Institute of Technology global model (at 1° horizontal resolution, with 23 vertical levels).

At the moment, we are not in a position to determine whether the explicit presence of mesoscale-eddy variability alters qualitatively the picture presented here. Our analysis of optimal forcing reveals that decadal remote response is most sensitive to forcing near the eastern boundaries in high latitudes, while mesoscale-eddy energy is largest near the western boundaries in midlatitudes. Furthermore, our calculations show a lack of sensitivity to the actual value of dissipation, also most important in the western boundary current, and to the dynamics in the model Antarctic circumpolar region, another eddy-rich region. We thus anticipate our results might be robust to the inclusion of eddy processes.

Acknowledgments. Funding for this research is provided by the U.S. Department of Energy. We benefited from discussions with Bill Young, and we thank Francesco Paparella for developing the numerical shallow water code employed here. The comments of the anonymous reviewers are gratefully acknowledged.

REFERENCES

Bryan, K., 1996: The steric component of sea level rise associated with enhanced greenhouse warming: A model study. *Climate Dyn.,* **12,** 545–555.

Cessi, P., and S. Louazel, 2001: Decadal oceanic response to stochastic wind forcing. *J. Phys. Oceanogr.,* **31,** 3020–3029.

——, and F. Primeau, 2001: Dissipative selection of low-frequency

modes in a reduced-gravity basin. *J. Phys. Oceanogr.*, **31,** 127–137.

Dewar, W., 1998: On ''too fast'' baroclinic planetary waves in the general circulation. *J. Phys. Oceanogr.*, **28,** 1739–1758.

Douglas, B., 2000: An introduction to sea level. *Sea Level Rise: History and Consequences*, B. C. Douglas et al., Eds., Academic Press, 1–11.

Farrell, B., and P. Ioannou, 1996: Generalized stability theory. Part I: Autonomous operators. *J. Atmos. Sci.*, **53,** 2025–2040.

Frankignoul, C., P. Müller, and E. Zorita, 1997: A simple model of the decadal response of the ocean to stochastic wind forcing. *J. Phys. Oceanogr.*, **27,** 1533–1546.

Fu, L.-L., and D. Chelton, 2001: Large-scale ocean circulation. *Satellite Altimetry and Earth Sciences: A Handbook of Techniques and Applications*, L.-L. Fu and A. Cazenave, Eds., Academic Press, 133–168.

Hsieh, W., and K. Bryan, 1996: Redistribution of sea level rise associated with enhanced greenhouse warming: A simple model study. *Climate Dyn.*, **12,** 535–544.

Huang, R., M. Cane, N. Naik, and P. Goodman, 2000: Global adjustment of the thermocline in response to deepwater formation. *Geophys. Res. Lett.*, **27,** 759–762.

Johnson, H., and D. Marshall, 2002: A theory for the surface Atlantic response to thermohaline variability. *J. Phys. Oceanogr.*, **32,** 1121–1132.

Kawase, M., 1987: Establishment of deep ocean circulation driven by deep-water production. *J. Phys. Oceanogr.*, **17,** 2294–2317.

Liu, Z., 1999: Forced planetary wave response in a thermocline gyre. *J. Phys. Oceanogr.*, **29,** 1036–1055.

Primeau, F., 2002: Long Rossby wave basin-crossing time and the resonance of low-frequency basin modes. *J. Phys. Oceanogr.*, **32,** 2652–2665.

Roemmich, D., J. Gilson, B. Cornuelle, and R. Weller, 2001: Mean and time-varying meridional transport of heat at the tropical/subtropical boundary of the north Pacific Ocean. *J. Geophys. Res.*, **106,** 8957–8970.

Sturges, W., and B. Hong, 2000: Decadal variability of sea level. *Sea Level Rise: History and Consequences*, B. C. Douglas et al., Eds., Academic Press, 165–180.